PCCP

PAPER

View Article Online
View Journal | View Issue

Cite this: *Phys. Chem. Chem. Phys.*, 2016, **18**, 2047

Thermal phase behavior and ion hopping in a 1,2,4-triazolium perfluorobutanesulfonate protic organic ionic plastic crystal†

Anirban Mondal,[a] Anurag Prakash Sunda[b] and Sundaram Balasubramanian*[a]

Received 23rd September 2015,
Accepted 7th December 2015

DOI: 10.1039/c5cp05701a

www.rsc.org/pccp

Critical aspects of thermal behavior and the electrolytic properties of solid-state Protic Organic Ionic Plastic Crystals (POIPCs) are unknown. We present molecular dynamics (MD) simulations on a perfect crystal and a vacancy model to probe such physical phenomena in POIPCs using 1,2,4-triazolium perfluorobutanesulfonate ([TAZ][pfBu]) as an example. The results show the existence of a rotator phase wherein the cations, although translationally ordered are disordered rotationally and exhibit a tumbling motion which significantly affects hydrogen bond lifetimes. van Hove correlation functions characterize the concerted hopping of ions (cation or anion) at 500 K. These results are substantiated by calculated free energy barriers (cation = 2.5 kcal mol^{-1} and anion = 6 kcal mol^{-1}) and suggest that proton and ion transport influenced by facile hydrogen bond dynamics in the rotator phase contribute to the solid-state conductivity of POIPCs.

1 Introduction

The thermal phase behavior of organic ionic plastic crystals (OIPCs) is crucial for their potential applicability as solid electrolytes in batteries, fuel cells and dye-sensitized solar cells.[1–17] The occurrence of one or more than one solid–solid phase transition in such plastic crystals is yet another reason that draws one's attention to investigate their structural characteristics. The varying dynamics of ions in different solid phases contribute critically to the electrolytic properties of pristine and alkali metal doped OIPCs.[18–23] Recently, Jin *et al.*[7] investigated the ion transport mechanism in a diethyl(methyl)(iso-butyl)phosphonium hexafluorophosphate ($[P_{1224}][PF_6]$) OIPC and showed that the tumbling motion of ions in its plastic phase aids faster ion diffusion. Further, molecular dynamics (MD) simulations by Forsyth and coworkers[24,25] on $[P_{1224}][PF_6]$ showed the presence of dynamical heterogeneity in the solid phase and a crankshaft motion around the alkyl groups (a methyl/ethyl group as the head and an iso-butyl group as the tail) in the plastic phase. Although plastic crystals exhibit long range translational order, orientational disorder can often set in at intermediate temperatures, which can enhance ion mobility.

Substantial progress has been made over the years in the research on OIPCs to demonstrate their potential as solid-state anhydrous electrolytes.[4,9] However, a molecular-level understanding of the phase behavior, the temperature-dependent disordering phenomenon and transport mechanisms in Protic Organic Ionic Plastic Crystal (POIPC) materials is yet to be explored. While the dominant contribution to electrical conductivity is protonic, at moderate temperatures, ion motion too has been implicated.[11] Experiments on a 1,2,4-triazolium perfluorobutanesulfonate ([TAZ][pfBu]) POIPC by Luo *et al.*[11] revealed the following features: up to 348 K, the crystal is stable, after which plastic deformation sets in. Ion rotation and likely diffusion happen in the range of 350–375 K which is followed by a transition to phase-I (375–430 K) which exhibits high conductivity with an activation energy of 0.38 eV. In this phase, proton hopping *via* the Grotthuss mechanism is believed to be operative. Within a narrow range of temperature above 430 K, both cations and anions are also mobile which is followed by the melt phase. Given the above, details of the molecular motion of ions in a perfect crystal and of vacancies need to be unravelled both by further experiments as well as microscopic simulations. While a study of proton transport is important, it will require *ab initio* MD simulations[26] and the likely inclusion of quantum effects on dynamics. Using empirical potential MD simulations, one can, however gain an understanding of the nature of phases as well as the mechanisms of the vehicular

[a] *Chemistry and Physics of Materials Unit, Jawaharlal Nehru Centre for Advanced Scientific Research, Bangalore 560064, India. E-mail: bala@jncasr.ac.in; Fax: +91 (80) 2208 2766; Tel: +91 (80) 2208 2808*

[b] *Materials Research Laboratory, Department of Chemistry, Central University of Haryana, Mahendergarh, Haryana 123029, India*

† Electronic supplementary information (ESI) available: Details of atomic site charge calculations, normal-mode analysis and estimation of ion hopping frequencies and jump diffusion coefficients are provided. Summary of cell parameters and non-exponential fit parameters for h-bond correlation functions is tabulated. Chemical structure of [TAZ][pfBu], change in volume with temperature, RDFs for various cation–anion sites, powder XRD patterns, VDOS, MSD of cation and anion, reaction coordinate for free energy calculation and additional figures are shown. See DOI: 10.1039/c5cp05701a

diffusion of ions. In this spirit, in the present work, we report results on the structures of the different thermal phases of a 1,2,4-triazolium perfluorobutanesulfonate ([TAZ][pfBu]) POIPC, obtained using such classical MD simulations. Significant changes in the cation–anion hydrogen bonding network[11] and a concomitant freedom from orientational order are seen in the plastic crystalline phase of this compound.

2 Simulation details

The chemical structure of [TAZ][pfBu] is presented in Fig. S1 of the ESI.† MD simulations of the perfect crystalline phase of this salt and a model containing one ion pair vacancy were performed using the LAMMPS program.[27] Initial cell parameters and atomic positions were taken from the experimentally determined crystal structure.[11] The size of the simulation cell was $6 \times 4 \times 1$ unit cells (2496 atoms). A description of the systems studied here is provided in Table S1 of the ESI.† The interaction parameters used to model the triazolium cation were taken from the work of Maginn and co workers[28] and for the anion they were taken from the work of Goddard *et al.*[29] The latter force field did not have charges on the sites which are crucial for the current study. Hence, the site charges on ions were determined *via* periodic density functional theory calculations performed using CP2K.[30] The results of such calculations yielded the valence electron density which was used as the input in the DDEC/c3 method to derive atomic site charges.[31,32] A distance cutoff of 12 Å was employed to calculate pairwise interactions in real space. The time-step used to integrate the equations of motion was 0.5 fs. The long-range interactions were evaluated using a PPPM solver with a precision of 10^{-5}. The calculated cell parameters at 100 K differed by less than 0.7% of their experimental values (see Table S2 of the ESI†), which suggests that the crystal structure was stable in the simulations when employing these force field parameters. Energy minimization was performed on the initial configuration. The configuration was then warmed to 300 K at a heating rate of 1 K per 50 ps in the constant-*NVT* ensemble. It was followed by an equilibration of 5 ns at 300 K. The equilibrated configuration was further heated up to 500 K at a rate of 1 K per 100 ps in the fully flexible isothermal–isobaric (*NPT*) ensemble. Coordinates were dumped every 10 K and a further equilibration of 4 ns was carried out in the fully flexible isothermal–isobaric (*NPT*) ensemble at each temperature. The cell parameters were taken from these runs. After the initial equilibration, a separate trajectory of 10 ns was generated at each temperature in the *NVT* ensemble to compute several equilibrium properties. The variation in the cell parameters and the change in the cell volume with temperature (at different phases) are displayed in Fig. 1 and 2, respectively. We present a discussion on the identification of different phases in Fig. 2 later.

Vacancy model simulations

The vacancy model required large supercell dimensions ($8 \times 6 \times 2$) consisting of 384 ion pairs (9984 atoms). One cation and anion was removed in order to create vacancy sites.

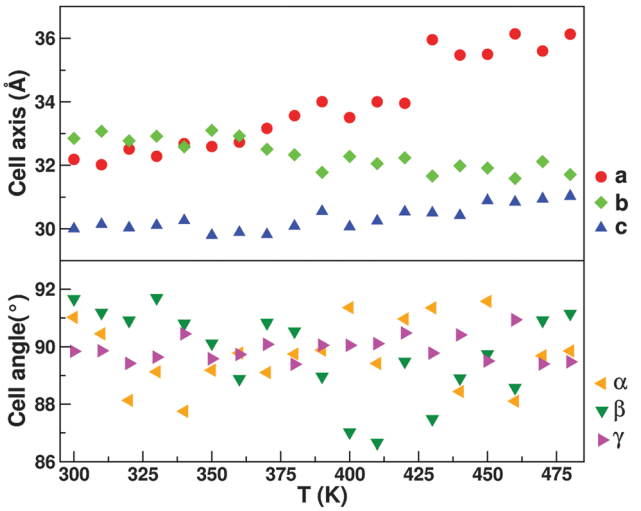

Fig. 1 Cell parameters as a function of temperature in a perfect crystalline model: cell axes (top) and cell angles (bottom). Standard deviations of the cell lengths and angles are 0.15 Å and 0.62° respectively.

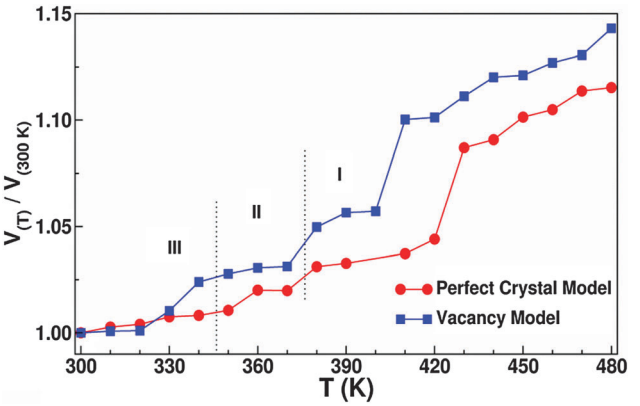

Fig. 2 Variation in the volume of a simulation cell with temperature.

An energy minimized configuration was used to perform a simulation in the *NVT* ensemble with a heating rate of 1 K per 50 ps to obtain a configuration at 500 K. It was followed by an another equilibration of 5 ns in the fully flexible *NPT* ensemble. The subsequent production trajectory was generated in the *NVT* ensemble for 100 ns to compute the dynamic properties. Other simulation details were kept similar to the perfect crystalline system.

Free energy calculations

To calculate the free energy barrier of the hopping of an ion to a neighbouring vacancy site, a large supercell ($8 \times 6 \times 2$) from the experimental[11] crystal structure was considered. Following energy minimization, MD simulations in the *NVT* ensemble were performed; later the system was warmed up to 500 K at a heating rate of 1 K per 50 ps. At 500 K, the system was equilibrated for over 5 ns in the fully flexible *NPT* ensemble. A further equilibration was carried out in the *NVT* ensemble for 1 ns. From this equilibrated configuration, a cation and anion

pair (non-adjacent) was chosen whose time average center of mass (COM) positions were calculated over a duration of 500 ps. The selected pair of ions was then removed and non-interacting dummy atoms were placed in their average COM positions, acting as reference locations for the vacancy site. The COMs of four ions (two cations and two anions) arbitrarily chosen so that they were situated far away from the chosen vacancy site were constrained such that the whole system cannot translate during the simulation. A colvar style "distance Z" was used in determining the free energy profile using the Adaptive Biasing Force (ABF) method.[33] The reaction coordinate (RC) was defined as the distance between the COM of an ion (cation or anion) and the COM of a dummy atom (see Fig. S2, ESI†). Typically, the closest ion to the vacancy site was chosen as the "hopping" ion. ABF forces were applied every 500 steps with a bin width of 0.2 Å. An average sampling ratio was around 4 after 5 ns between the highest and lowest points. The same procedure was applied to five different initial configurations for both ion types. The free energy profiles were calculated from these five initial configurations and are presented in Fig. S3 (ESI†). The mean free energy profile is presented and discussed later.

The effect of temperature on the vibrational spectrum was investigated through normal-mode analysis (NMA) at the harmonic level. For this, configurations collected from the classical MD trajectory at different temperatures were energy minimized in LAMMPS.[27] Later, the Hessian matrix (second derivative of the potential energy with respect to the atom coordinates) of such configurations was constructed using a normal-mode analysis code developed earlier by our group.[34] Within the harmonic approximation, diagonalization of this matrix yields eigenvectors which are proportional to the atomic displacements of different modes. The complete details of the charge calculations and normal-mode analysis (NMA) are provided in the ESI.†

3 Results and discussion

The structural characteristics of [TAZ][pfBu] at different temperatures were examined through cation–anion radial distribution functions (RDFs) (see Fig. S4 of the ESI†). The H_N–O and H_C–O RDFs show that the strong N–H···O and weaker C–H···O hydrogen bonding interactions are not much influenced by temperature. The number of H_N atoms within the first solvation shell of the oxygen atoms of the anion decreases with increasing temperature, shown in Fig. 3. As there are three hydrogen bonding sites on the anion and only two on the cation, the latter's rotation at intermediate temperatures allows the breakage of existing h-bonds and the formation of new ones. In this manner, every oxygen site on the anion participates in hydrogen bonding, creating a dynamic 3-dimensional hydrogen bonding network. The overall decrease in the coordination number suggests the presence of disorder at higher temperature. While the ion–ion RDFs at high temperature retain most features of those at low temperatures, a few critical shoulders

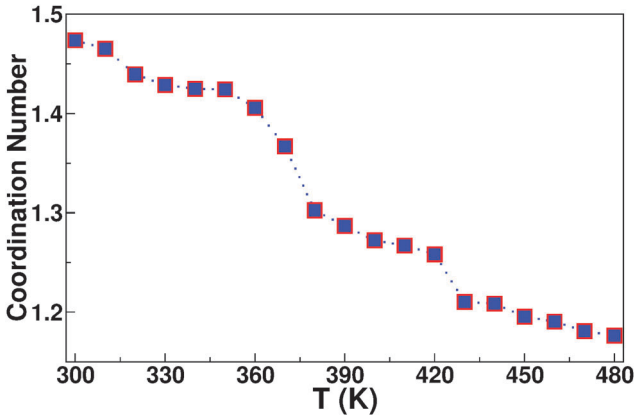

Fig. 3 Coordination number of the cation's N–H hydrogen (H_N) around the anion's oxygen as a function of temperature.

(sub-peaks) are missing, pointing to a loss of a certain degree of crystallinity. Crucially, the triazolium rings are seen to be misoriented with increasing temperature, although they retain their lattice positions (Fig. S5 of the ESI†). Such an intermediate phase between 380 K and 430 K can thus be called the rotator phase.

Ring plane rotational correlation ($C(t)$)

The rotational dynamics of the cation was investigated using the time autocorrelation function of its ring normal, $C(t)$ defined as,

$$C(t) = \langle \vec{R}_i(t) \cdot \vec{R}_i(0) \rangle \quad (1)$$

where $\vec{R}_i(t)$ is the normal vector corresponding to each 1,2,4-triazolium ring plane at time t and the function is averaged over the initial times and cation indices. Fig. 4 shows that $C(t)$ does not decay much at 300 K. At low temperature (phase III, Fig. 2), the ring planes of the cations are oriented in a perfect manner as shown in Fig. 5a. Between 360 K and 380 K, the rate of decay increases sharply (phase II, Fig. 2). Above 430 K, (phase I, Fig. 2)

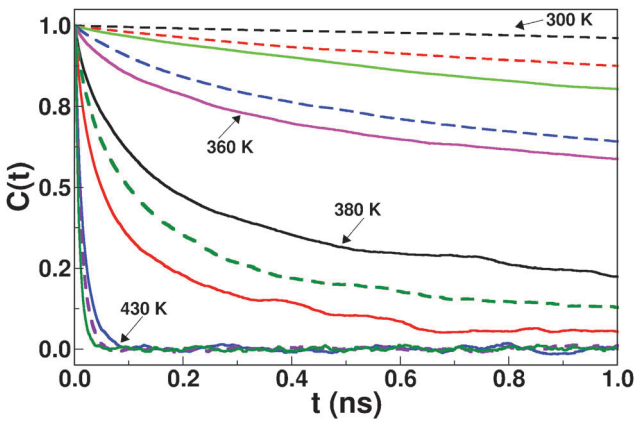

Fig. 4 Auto time correlation function of the ring plane normal of the cation at different temperatures. Only a few lines are marked with temperature for the sake of clarity, unmarked lines correspond to intermediate temperatures.

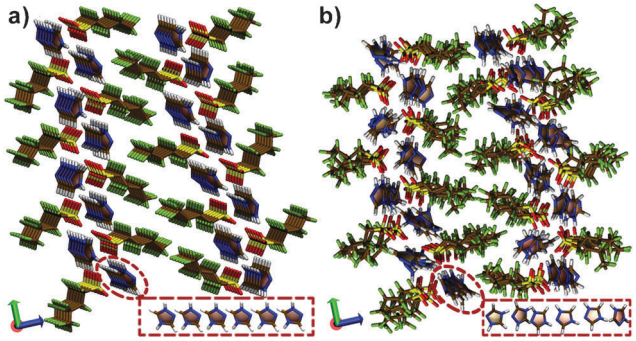

Fig. 5 Snapshots of ([TAZ][pfBu]) from *NVT* production runs at (a) 330 K, and (b) 380 K [carbon – ochre, nitrogen – blue, oxygen – red, fluorine – green, and sulfur – yellow (Licorice view)].

the correlation function decays to zero within 0.05 ns. The cations in the lattice lose their orientational rigidity in the temperature range of 330–380 K, above which they are free to rotate which is also seen in Fig. 5 and Fig. S5 of the ESI.† Thus, the orientational order between the 1,2,4-triazolium ring planes is decorrelated at higher temperature. The ring starts rotating above 350 K and tumbles at ~430 K.

The distribution of the angle between the ring planes of neighboring cations was calculated at different temperatures. Fig. 6 shows it to be sharply peaked at low temperatures with values around ±1, implying the parallel orientation of such planes. At high temperatures, a nearly uniform distribution is seen which points to complete orientational disorder. The onset of this disorder can be captured by plotting the area under the curve (A) (between cos(θ) values of −1.0 to −0.7 and 0.7 to 1.0) against temperature as shown in the inset of Fig. 6. Its behavior is similar to that of the dependence of volume on T (see Fig. 2 and Fig. S6 of the ESI†), however the transitions are more evident. The observed discontinuities in both this area and the cell volume at the phase transitions are in excellent agreement with the experiments,[11] as expected for the three phases (phases III, II and I) of a [TAZ][pfBu] POIPC,

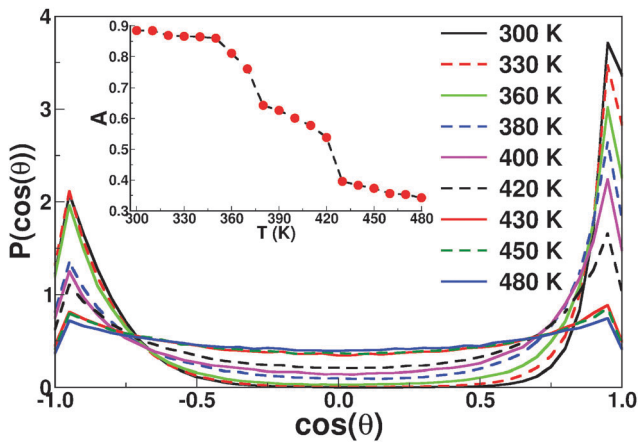

Fig. 6 Distribution of the angle between the ring planes of neighboring cations. Inset: Area under the distribution, for the regions $|\cos\theta| > 0.7$ *versus* temperature.

although the transition temperatures seen in the simulations are higher, due to superheating effects. Thus, in the simulations, the crystal is in the rotator phase at temperatures higher than 420–430 K too, and phase I of the simulations is a metastable one.

Further, the vibrational density of states (VDOS) of [TAZ][pfBu] was calculated at various temperatures from the Fourier transform of the velocity time autocorrelation function of the ions (see Fig. S8 of the ESI†). An increase in temperature results in the softening of modes present below 100 cm^{-1} and around 700 cm^{-1}. The former can be assigned to the librations of cations and the latter to the out-of-plane motion of the N–H protons in the triazolium cation (see Fig. 7). Rotational disorder at higher temperature facilitates cation mobility and thus causes the change in spectral behaviour. These observations reproduce the experimental results of Luo *et al.*[11] using a [TAZ][pfBu] POIPC.

The dynamics of breakage and re-formation of the cation–anion hydrogen bonds can be studied through time correlation functions. Two such TCFs, $S_{HB}(t)$ and $C_{HB}(t)$ can be defined,[35–38] the former providing a measure of the life time of a hydrogen bond while the latter measures the same, but allows for the reformation of a hydrogen bond between the same donor–acceptor pair.

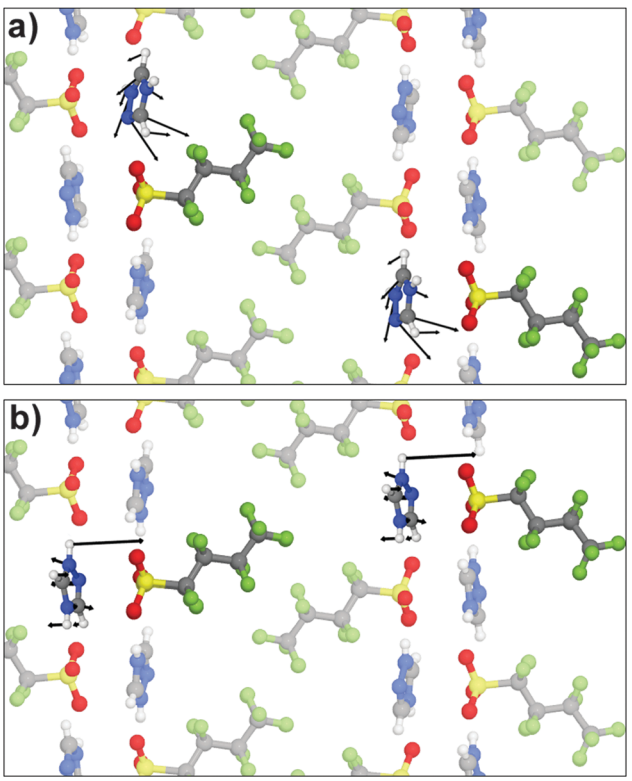

Fig. 7 Atomic displacements obtained from the normal mode analysis of a crystalline POIPC. Two modes are shown for illustrative purposes. (a) Librational mode of the triazolium cation at 100 cm^{-1}, and (b) out-of-plane motion of the N–H proton of the triazolium cation at 715 cm^{-1}. Only a few ions from the modeled crystal are shown for the sake of clarity. Arrows are atomic displacements and are scaled by an arbitrary factor for better visualization. Color scheme: N – blue, C – gray, H – white, S – yellow, O – red, and F – green.

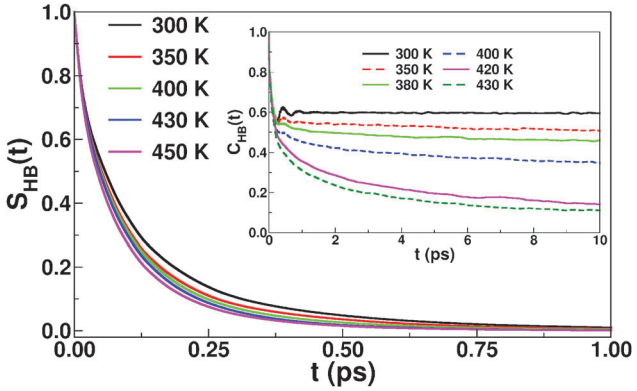

Fig. 8 Relaxations of the $S_{HB}(t)$ and $C_{HB}(t)$ (see inset) h-bond lifetime correlation function, for N–H···O hydrogen bonding in a POIPC.

The geometric criteria to determine the presence of a h-bond and the definitions of the h-bond life time correlation functions are provided in the ESI.†

Fig. 8 displays the decay of $S_{HB}(t)$ and $C_{HB}(t)$ at different temperatures. $S_{HB}(t)$ relaxes quite fast even at 300 K due to the fast bond vibrational and librational motions of the ions. With increasing temperature, the decay rate increases. However, $C_{HB}(t)$ exhibits rapid oscillations at 300 K and decays to a constant value. The long time value of $C_{HB}(t)$ decreases with increasing temperature. At low temperatures, the probability for the reformation of a h-bond is high and the non-zero asymptotic value of $C_{HB}(t)$ reflects this fact. At temperatures between 400 K and 430 K, this function decays slowly. The lifetime correlation functions were fitted to multi-exponential functions so as to obtain a mean relaxation time. The fit parameters are tabulated in Tables S3 and S4 of the ESI.† The mean lifetime obtained from $S_{HB}(t)$ is around 100 fs. Anion rotation has been suggested to assist proton hopping in a POIPC crystal.[11] The short lifetime of the h-bond TCF in the plastic crystalline phase of this POIPC supports this mechanism. Further, the temperature dependence of the hydrogen bond lifetime and rotational time are compared in Fig. 9 and interestingly, both of them were found to obey an Arrhenius behaviour. A linear fit of the time constants to inverse

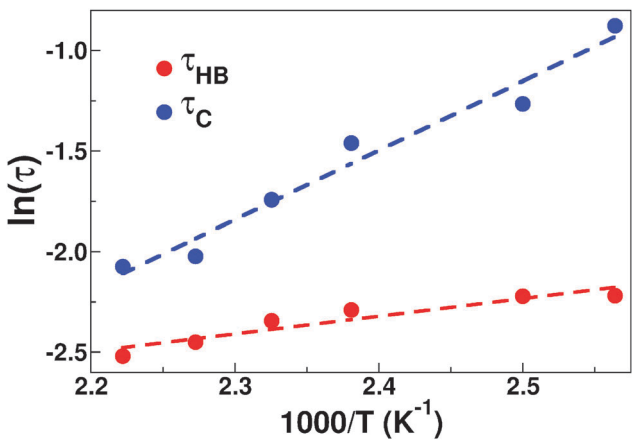

Fig. 9 Temperature dependence of the hydrogen bond lifetime (τ_{HB}) and rotational time (τ_C). Dashed lines are best fits.

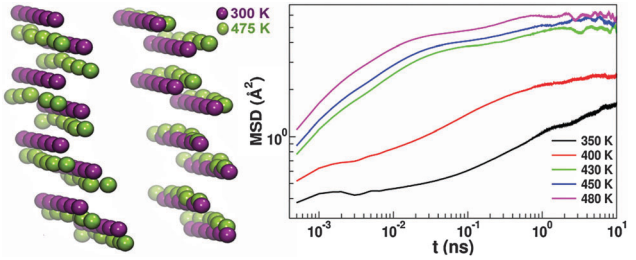

Fig. 10 Time averaged positions of the cation ring center at 300 K and 475 K (left); and its mean square displacement.

temperature yields the associated activation energy of individual events. As expected, the faster hydrogen bond lifetime possess a lower activation barrier (1.75 kcal mol^{-1}) than the slower rotational time (6.78 kcal mol^{-1}).

In the IL crystal, each ion is surrounded by its counterions forming a cage. Time averaging of ion positions permits the visualization of the underlying translational order in the crystal due to the effective "removal" of vibrational disorder. The same is shown in Fig. 10. The average positions of the ring center at 300 K and 475 K are nearly identical, implying the invariance of translational order with temperature over this range. The mean squared displacement (MSD) of the cations is also shown. After the initial ballistic motion (~0.2–0.7 ps), the MSDs of the cations exhibit a plateau region (MSD ~ 0.3–0.4 Å^2) due to the "cage". The plateau is very clearly seen at low temperatures. The time over which an ion is trapped inside a cage is different for cations and anions. The cations escape from the cage sooner due to their smaller size and rotational barrier,[24] compared to that of the anion (see Fig. S9 of the ESI† which presents the MSD of the cation and anion at various temperatures).

The van Hove self-correlation functions identify the nature of the translation of ions as either due to hopping or diffusion.[39] Even within the diffusive regime, they can aid in identifying dynamical heterogeneity.[25,40–42] The functions for the ions were calculated at 500 K, 550 K and 600 K between a 0.25 to 1 ns time regime and are shown in Fig. 11. The first peak position for anions is slightly larger than that for cations. At 550 K, a short second peak at around 6 Å (first neighboring distance of ions) is seen at a time duration of 1 ns. The peak height grows gradually between 550 K and 600 K within a 0.75 ns to 1 ns time scale. As discussed earlier, the translational motion of ions is restricted due to the formation of a cage by the counterion. The emergence of the second peak in $G_s(r,t)$ implies cation hopping. In a perfect crystal (as is the case studied here), the migration of ions is possible only due to fluctuations in their environment. In the present instant, the latter is aided by rotational disorder as discussed earlier. Rotational disorder aids in the migration of ions to their neighboring sites through the available free space due to structural relaxation. The cations attempting to hop to a neighboring site to later revert back to their original position, were also observed in movies of the trajectories.

Ion transport in a crystalline solid state is primarily aided through defects, the chief of which would be vacancies. Their concentration would increase with temperature. It is thus

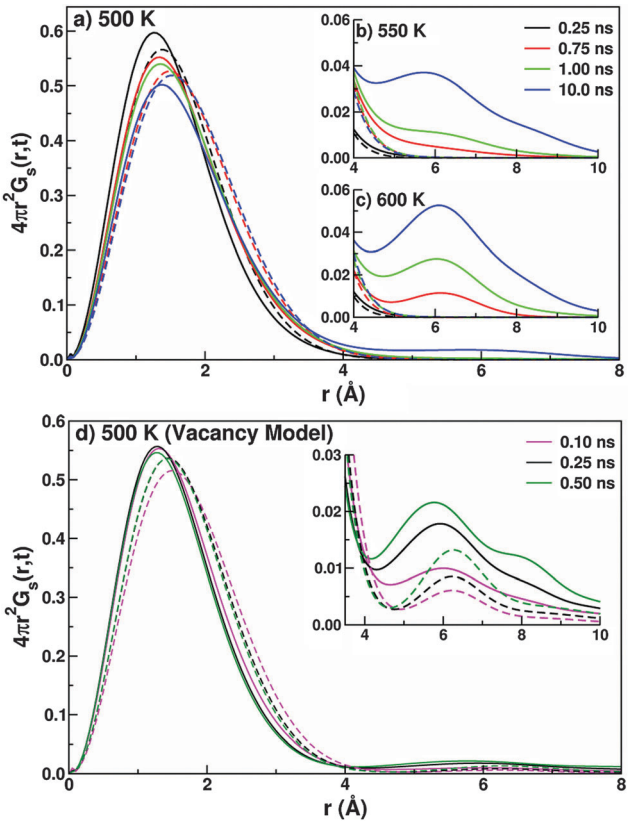

Fig. 11 Self part of the van Hove correlation functions calculated for a perfect crystalline lattice from MD simulations at (a) 500 K, (b) 550 K and (c) 600 K, and using the vacancy model at (d) 500 K (solid line – for the cation and dashed line – for the anion).

important to study the ion hopping phenomenon in the presence of vacancies. To this end, we have performed simulations of the crystal at 500 K which contained 384 ion pairs and one vacancy each of a cation and anion. The van Hove correlation function calculated at 500 K for such a vacancy model shows the hopping of the cation taking place within a 1 ns time scale which was not observed in the perfect crystal (see Fig. 11). Thus, as expected, ion hopping occurs at a much lower temperature due to the presence of vacancies. The decay of the ring plane normal rotational correlation is much faster in the presence of vacancies compared to the perfect crystal (see Fig. S10 of the ESI†) which suggests that rotational disorder occurs at a lower temperature due to the vacancies.

Fig. 12(a)–(c) is a pictorial view depicting the concerted hopping of the cations which results in a one-dimensional vacancy motion along the crystallographic *b*-axis. Similar to the cations, a concerted hopping of the anions is shown in Fig. S11 of the ESI.† The qualitative observations showed that the hop rate for the cations was higher than that for the anions. We have performed free energy calculations at 500 K to obtain the barrier associated with the hopping of ions. The calculated activation energy barrier is found to be 2.5 kcal mol^{-1} and 6.0 kcal mol^{-1} for cations and anions, respectively (see Fig. 12(d)). Thus, a large energy barrier restricts the hopping of the anions. Free energy calculations at a lower temperature of 400 K, but still within phase I, yield larger barrier heights of 4.5 and 9.2 kcal mol^{-1} for the two ions. The activation (E_a) barrier obtained from the ionic conductivity experiments in phase I (373–430 K) was found to be 8.77 kcal mol^{-1}.[11] Although the results from the simulations are able to predict the order of magnitude of E_a, differences exist between the simulations and the experiments.[11] This could be due to the fact that the measured ionic conductivity in the experiments is primarily protonic in nature, while the calculated activation energy from simulations is solely from individual ion motion *i.e.* cation and anion movement. Further, an estimation of ion hopping frequencies and the corresponding jump diffusion coefficients was obtained using these free energy barriers associated with the motion of cations and anions. A detailed discussion of the same is provided in the ESI.†

4 Conclusions

In conclusion, we have identified the existence of a rotator phase in a [TAZ][pfBu] POIPC. It is characterized by the decorrelation of the orientation of cation ring planes. In the plastic crystalline phase, ion rotation leads to a short life-time of the N–H···O hydrogen bond. The same has been characterized *via* h-bond lifetime correlation functions. The rotational disorder also allows for the hopping of ions at higher temperatures. The disorder and consequent ion hopping are accelerated due to vacancies in the crystal, and thus occur at lower temperatures (by at least 20 K) than in a perfect crystal. As the heating

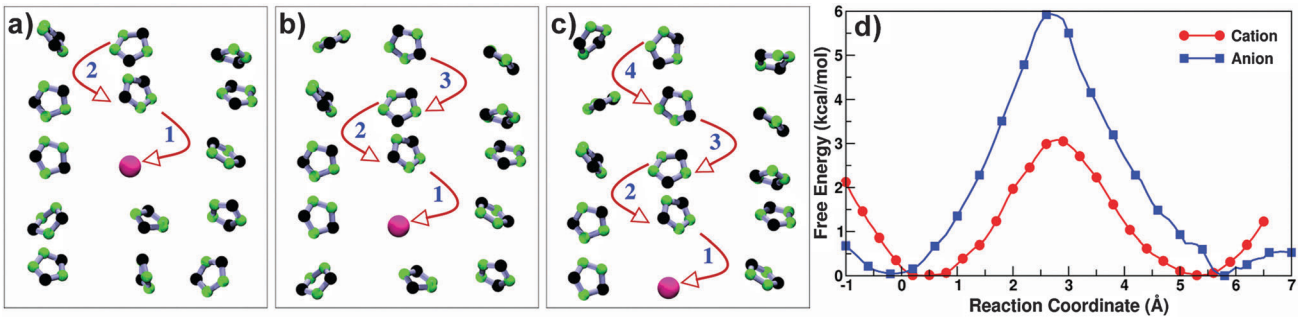

Fig. 12 (a–c) Concerted hopping of the cations and (d) calculated free energy profiles for the motion of the cation and anion at 500 K. Estimated standard error in the mean in the simulated free energy is around 0.22 kcal mol^{-1}.

rates employed here are much higher than those used in experiments, superheating is likely; the same would be reflected in the higher values of the temperatures of phase transitions in simulations when compared to experiments. One-dimensional vacancy motion has been delineated and the free energy barrier for ion hopping has been estimated to be 2.5 and 6.0 kcal mol^{-1} for cations and anions, respectively. It will be interesting to extend these atomistic simulations to investigate the diffusion of additional ionic species like small alkali ions in such POIPCs, as well as to study proton diffusion using *ab initio* MD methods.

Acknowledgements

AM thanks JNCASR for financial support. AM thanks Karteek Kumar Bejagam for assistance in free energy calculations. APS acknowledges DST for the INSPIRE Faculty Award (DST/INSPIRE/IFA-14-MS31) and the Central University of Haryana for financial support. SB thanks the Sheikh Saqr Laboratory, JNCASR for a senior fellowship.

References

1 D. R. MacFarlane, J. Huang and M. Forsyth, *Nature*, 1999, **402**, 792–794.
2 P.-J. Alarco, Y. Abu-Lebdeh, A. Abouimrane and M. Armand, *Nat. Mater.*, 2004, **3**, 476–481.
3 S. J. Pas, J. M. Pringle, M. Forsyth and D. R. MacFarlane, *Phys. Chem. Chem. Phys.*, 2004, **6**, 3721–3725.
4 J. M. Pringle, P. C. Howlett, D. R. MacFarlane and M. Forsyth, *J. Mater. Chem.*, 2010, **20**, 2056–2062.
5 V. Armel, D. Velayutham, J. Sun, P. C. Howlett, M. Forsyth, D. R. MacFarlane and J. M. Pringle, *J. Mater. Chem.*, 2011, **21**, 7640–7650.
6 V. Armel, M. Forsyth, D. R. MacFarlane and J. M. Pringle, *Energy Environ. Sci.*, 2011, **4**, 2234–2239.
7 L. Jin, K. M. Nairn, C. M. Forsyth, A. J. Seeber, D. R. MacFarlane, P. C. Howlett, M. Forsyth and J. M. Pringle, *J. Am. Chem. Soc.*, 2012, **134**, 9688–9697.
8 Q. Li, X. Chen, J. Zhao, L. Qiu, Y. Zhang, B. Sun and F. Yan, *J. Mater. Chem.*, 2012, **22**, 6674–6679.
9 J. M. Pringle, *Phys. Chem. Chem. Phys.*, 2013, **15**, 1339–1351.
10 S. Li, L. Qiu, C. Shi, X. Chen and F. Yan, *Adv. Mater.*, 2014, **26**, 1266–1271.
11 J. Luo, A. H. Jensen, N. R. Brooks, J. Sniekers, M. Knipper, D. Aili, Q. Li, B. Vanroy, M. Wubbenhorst, F. Yan, L. Van Meervelt, Z. Shao, J. Fang, Z.-H. Luo, D. E. De Vos, K. Binnemans and J. Fransaer, *Energy Environ. Sci.*, 2015, **8**, 1276–1291.
12 Q. Li, J. Zhao, B. Sun, B. Lin, L. Qiu, Y. Zhang, X. Chen, J. Lu and F. Yan, *Adv. Mater.*, 2012, **24**, 945–950.
13 D. R. MacFarlane and M. Forsyth, *Adv. Mater.*, 2001, **13**, 957–966.
14 L. Jin, P. C. Howlett, J. M. Pringle, J. Janikowski, M. Armand, D. R. MacFarlane and M. Forsyth, *Energy Environ. Sci.*, 2014, **7**, 3352–3361.
15 P. Wang, Q. Dai, S. M. Zakeeruddin, M. Forsyth, D. R. MacFarlane and M. Grätzel, *J. Am. Chem. Soc.*, 2004, **126**, 13590–13591.
16 J. Golding, N. Hamid, D. R. MacFarlane, M. Forsyth, C. Forsyth, C. Collins and J. Huang, *Chem. Mater.*, 2001, **13**, 558–564.
17 M. Patel and A. J. Bhattacharyya, *Energy Environ. Sci.*, 2011, **4**, 429–432.
18 L. Jin, S. de Leeuw, M. V. Koudriachova, J. M. Pringle, P. C. Howlett, F. Chen and M. Forsyth, *Phys. Chem. Chem. Phys.*, 2013, **15**, 19570–19574.
19 M. Forsyth, T. Chimdi, A. Seeber, D. Gunzelmann and P. C. Howlett, *J. Mater. Chem. A*, 2014, **2**, 3993–4003.
20 F. Chen, J. M. Pringle and M. Forsyth, *Chem. Mater.*, 2015, **27**, 2666–2672.
21 C. Shi, S. Li, W. Zhang, L. Qiu and F. Yan, *J. Mater. Chem. A*, 2013, **1**, 13956–13962.
22 Q. Dai, D. R. MacFarlane, P. C. Howlett and M. Forsyth, *Angew. Chem., Int. Ed.*, 2005, **44**, 313–316.
23 K. Romanenko, J. M. Pringle, L. A. O'Dell and M. Forsyth, *Phys. Chem. Chem. Phys.*, 2015, **17**, 18991–19000.
24 F. Chen, L. Jin, S. W. de Leeuw, J. M. Pringle and M. Forsyth, *J. Chem. Phys.*, 2013, **138**, 244503.
25 F. Chen, S. W. de Leeuw and M. Forsyth, *J. Phys. Chem. Lett.*, 2013, **4**, 4085–4089.
26 L. Vilčiauskas, M. E. Tuckerman, G. Bester, S. J. Paddison and K.-D. Kreuer, *Nat. Chem.*, 2012, **4**, 461–466.
27 S. Plimpton, *J. Comput. Phys.*, 1995, **117**, 1–19.
28 C. Cadena and E. J. Maginn, *J. Phys. Chem. B*, 2006, **110**, 18026–18039.
29 S. S. Jang, V. Molinero, T. Cagin and W. A. Goddard, *J. Phys. Chem. B*, 2004, **108**, 3149–3157.
30 J. Hutter, M. Iannuzzi, F. Schiffmann and J. VandeVondele, *Wiley Interdiscip. Rev.: Comput. Mol. Sci.*, 2014, **4**, 15–25.
31 T. A. Manz and D. S. Sholl, *J. Chem. Theory Comput.*, 2010, **6**, 2455–2468.
32 T. A. Manz and D. S. Sholl, *J. Chem. Theory Comput.*, 2012, **8**, 2844–2867.
33 E. Darve, D. RodríguezGómez and A. Pohorille, *J. Chem. Phys.*, 2008, **128**, 144120.
34 M. Krishnan and S. Balasubramanian, *Phys. Rev. B: Condens. Matter Mater. Phys.*, 2003, **68**, 064304.
35 D. Rapaport, *Mol. Phys.*, 1983, **50**, 1151–1162.
36 A. Luzar and D. Chandler, *Nature*, 1996, **379**, 53.
37 A. Chandra, *Phys. Rev. Lett.*, 2000, **85**, 768–771.
38 S. Balasubramanian, S. Pal and B. Bagchi, *Phys. Rev. Lett.*, 2002, **89**, 115505.
39 S. Balasubramanian and K. J. Rao, *J. Phys. Chem.*, 1994, **98**, 10871–10880.
40 S. S. Sarangi, W. Zhao, F. Müller-Plathe and S. Balasubramanian, *ChemPhysChem*, 2010, **11**, 2001–2010.
41 S. M. Urahata and M. C. C. Ribeiro, *J. Phys. Chem. Lett.*, 2010, **1**, 1738–1742.
42 H. Liu and E. Maginn, *J. Chem. Phys.*, 2011, **135**, 124507.